MEID Design Methodology for Object-Wall-Collision Problems

Yohei Kushida[1], Hiroaki Umehara[2], Susumu Hara[3] and Keisuke Yamada[4]

[1]Department of Mechanical Science and Engineering, Graduate School of Engineering, Nagoya University, Japan

[2]Center for Information and Neural Networks (CiNet), National Institute of Information and Communications Technology, and Osaka University, Japan

[3]Department of Aerospace Engineering, Graduate School of Engineering, Nagoya University, Japan

[4]Department of Mechanical Engineering, Faculty of Engineering Science, Kansai University, Japan

Corresponding author:

Youhei Kushida, Department of Mechanical Science and Engineering, Nagoya University, Furo-cho, Chikusa-ku, Nagoya, 464-8603, Japan.

Email: y.kushida.0411@gmail.com

Abstract

Momentum exchange impact dampers (MEIDs) were proposed to control shock responses of mechanical structures. They were applied to reduce floor shock vibrations and control lunar/planetary exploration spacecraft landings. MEIDs are required to control an object's velocity and displacement, especially for applications involving spacecraft landing. Previous studies verified numerous MEID performances through various types of simulations and experiments. However, previous studies discussing optimal design methodology for MEIDs are limited. This study explicitly derived the optimal design parameters of MEIDs, which controls the controlled object's displacement and velocity to zero in one-dimensional motion. Additionally, the study derived sub-optimal design parameters to control the controlled object's velocity within a reasonable approximation to derive a practical design methodology for MEIDs. The derived sub-optimal design methodology could also be applied to MEIDs in two-dimensional motion. Furthermore, simulations conducted in the study verified the performances of MEIDs with optimal/sub-optimal design parameters.

Keywords

MEID; momentum exchange; shock; vibration; spacecraft; landing

1. Introduction

The control of shock responses in applications involving floor vibrations and landing of lunar/planetary exploration spacecraft is a very important engineering problem. Floor vibration is a common problem in industrial and environmental areas (Nyawako,

2015). The large vibration response and transmitted force in forging machines decreases machining accuracy and causes vibration pollution to the surroundings. Floor vibrations in bank buildings due to shock excitation by human activities can cause floor vibrations and noises to the ceiling of lower rooms. Fundamental researches of shock response analyses discussed an impact on a bar(Oda and Hukatsu, 1979), for example. A vibration reduction methods using additional masses, which are called impact dampers were studied by Thomas MD and Sadek MM (1974), which a free mass can vibrate within end stops which are fixed to a vibrating system. Typical parameters of the impact dampers are mass ratio, coefficient of restitution and gap size of the free mass (Bapat CN and Sanker S, 1985a; Duncan MR *et al*., 2005; Cheng J and Xu H, 2006). Resilient type free mass case was also studied to concern noise issue (Cheng CC and Wang JY, 2003). As further expansion, multiple free masses case (Bapat CN and Sanker S, 1985b) and multi-particle type impact damper (Saeki M, 2005) was also discussed. Such devices using the similar mechanism as MEID is not only in mechanical engineering, but also in civil engineering (Lu Z, 2011a; Lu Z, 2011b; Lu Z, 2014; Lu Z, 2016a; Lu Z, 2016b; Lu Z, 2017). These studies mainly focuses on suppressing periodical motion by dissipation of the shock between the free mass and a vibrating system. From the viewpoint of controlling the initial shock response, momentum exchange impact dampers (MEIDs) were proposed (Son *et al*., 2007). The billiards principle shown in Fig. 1 can be used to explain the mechanisms of a MEID, wherein the MEID reduces the shock response of an object by exchanging the momentum of the object with the MEID's own momentum. This model is also termed as the Newton's cradle (Dondo and Noborio, 2008).

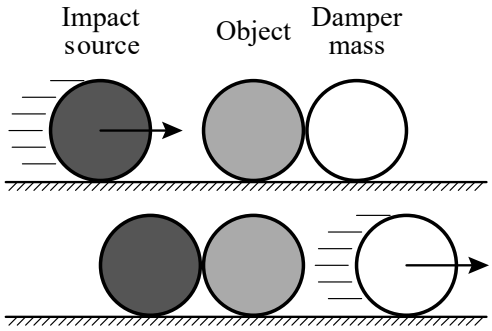

Figure 1. Conceptual diagram of a MEID.

According to the type of mechanism employed for momentum transfer, MEIDs can be classified into three types. The first MEID type is the passive MEID (PMEID), which is composed of only passive elements such as linear springs and dashpots (Son *et al*., 2007; Son *et al*., 2008a). The second MEID type is the active MEID (AMEID), which includes active actuators. AMEID can greatly reduce the influence of shock responses because of its effective momentum exchange through the actuators when compared to PMEID. Previous studies proposed AMEID as a solution for the floor shock response control problem and discussed its effectiveness through simulations (Son *et al*., 2008b; Son *et al*., 2010).

The application of MEID involving landing of lunar/planetary exploration spacecraft was discussed by extant studies (Hara *et al*., 2011; Kushida *et al*, 2013a). Figure 2 shows a schematic representation of a spacecraft-landing problem. The spacecraft-

landing mission necessitates the reusability of the landing gear (Hufenbach *et al*., 2013). Previously, aluminum-foam-based landing gear has been proposed as a representative landing gear (Kitazono *et al*., 2010). This involved plastic deformation of the landing gear such that there was no reusability. Also, the landing problem needs to control a spacecraft's attitude before tripping of the spacecraft. Thus, the method which can control the first impact is primarily important rather than periodical vibration control methods. From this viewpoint, MEID is an important candidate for spacecraft landing gear. Spacecraft rebound and tripping are the most important problems in a lunar/planetary exploration mission. Thus, when MEIDs are used to solve the landing problem, the focus should be on reducing displacement and velocity of a spacecraft and not the transferred force.

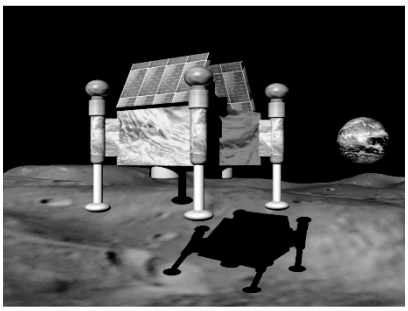

Figure 2. Schematic representation of a spacecraft landing on the moon (Kushida, 2013; Kushida and Hara, 2015; Kushida *et al*., 2013a, 2013b).

The third MEID type is an active/passive hybrid MEID (HMEID), which was suggested in order to increase the effectiveness of PMEID with small actuators in cases in which it is difficult to install a sufficiently strong actuator (Kushida *et al*, 2013b). HMEID uses actuators in combination with the passive elements. Additionally, Hara *et al*. (2012) discussed the mechanism that damper masses were thrown in the impact direction and opposite direction to further improve the shock control effectiveness of HMEIDs.

It is necessary to prevent tripping during the landing of a lunar/planetary exploration spacecraft. Thus, MEIDs are required to reduce both translational motion and rotational motion. MEID design methodology for two-dimensional motion is also important to reduce both translational and rotational motion. Kushida (2013) and Watanabe *et al*. (2014) discussed MEID design examples to prevent spacecraft tripping. Kushida and Hara (2015) attempted to generalize and derive MEID parameters that could suppress both translational and rotational motions. However, brute-force simulations were used to calculate the parameters. Additionally, theoretical analyses were not performed on the parameters.

Even in the restricted one-dimensional case without rotational motion, the optimal parameter for controlling translational motion was derived by simulation-based calculation. Several studies examined MEID responses in one-dimensional motion. Fundamental analysis for reducing a controlled object's rebound in a single-axis falling type problem was discussed (Kushida *et al.*, 2013a). This involved the optimization of a single parameter, namely spring stiffness that connects the controlled object and

damper mass. Both simulations and experiments were used to verify the optimization (Kushida *et al*., 2013b). However, the parameter was not optimized explicitly.

Aiming at systematic design of MEIDs, this study theoretically derived MEID design methodology for an object that collides with a wall. The design aim included controlling the displacement and velocity of the object after collision. This problem is termed as the object-wall-collision problem in this study. Although this is a widely known phenomenon that is discussed as multiple ball collision on a wall or ball-chain collision problem (Herrmann *et al*., 1981, 1982). Furthermore, this study models not only head-on collision but also collision that induces rotational motion in lunar/planetary exploration spacecraft landing.

This study offers the two advantages. First, the study described dynamics of a MEID model with one-dimensional motion and used theoretical analysis to derive the optimal parameters of the model, which controlled both displacement and velocity of the object. Then, sub-optimal parameters that control the object's velocity were derived as a practical value. The study classified vibration modes induced by a shock and focused on a representative mode that corresponded to an actual collision phenomenon. The analyses for the sub-optimal parameter were performed with a reasonable approximation based on energy and momentum conservation laws. Moreover, the robustness of MEIDs designed with the optimal parameters and sub-optimal parameters were compared with each other. Second, the study described two-dimensional dynamics of MEIDs by using energy, momentum, and angular momentum conservation laws and located sub-optimal parameters that controlled the object's translational and rotational velocity. The robustness of MEIDs designed with the sub-optimal parameters is confirmed by the assistance of numerical simulations.

2. MEID design for one-dimensional motion

The most fundamental problem of MEIDs include one-dimensional motion collision problem and MEID design methodology for the colliding body. This section aims to derive the design methodology for the one-dimensional problem. Kushida *et al*. (2013a) studied a similar problem with a spacecraft-landing model, which was termed the single-axis falling-type problem. However, the problem did not concretely clarify the contacting phase in which body mass was subjected to an impact force. The present study analytically analyzed the phase to derive obvious optimal design parameters. First, optimal design parameters that controlled both the object's displacement and velocity to zero were derived. Second, sub-optimal parameters that controlled the object's velocity to zero were discussed.

2.1. Dynamics of MEID model with one-dimensional motion

Figure 3 shows the MEID model with one-dimensional motion. This model consists of two masses, m and M, corresponding to the damper mass and the body mass, respectively. Their displacements are described by $x(t)$ and $X(t)$, respectively. Additionally, k denotes the contact stiffness between the damper mass and body mass and K denotes the body mass and wall. To focus on the first impact control rather than periodical motion, the important parameters for this paper are mass and spring constant, rather than damping coefficient. Also, to simplify the following analyses and obtain the analytical solution of the model, this paper does not consider energy dissipation which

is described by dashpots. The collision problem of this model was termed as the object-wall-collision problem in one-dimensional motion.

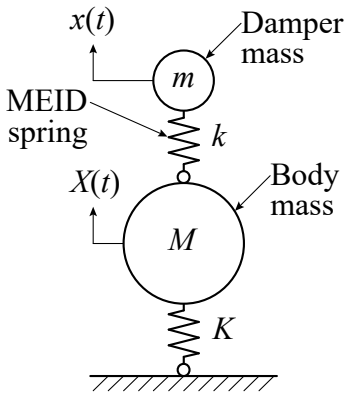

Figure 3. MEID model of a one-dimensional collision.

The representative collision phenomenon of the model is schematically depicted in Fig. 4. Here, "collision," $t = t_0 = 0$, is defined as the first moment at which the body mass touches the wall. It corresponds to the moment when the absolute displacements of the body mass and damper mass become zero [$X(t_0) = x(t_0) = 0$]. The velocities of the body mass and the damper mass at this moment are v_0 [$V(t_0) = v(t_0) = 0$]. Thereafter, the body mass immediately leaves the wall and the displacement becomes 0 again [$X(t_b) = 0$]. This moment is defined as "body-separation," [$t = t_b$]. After body-separation, the wall spring is eliminated and the body is separated from the wall. Subsequently, the displacement of the damper mass becomes equal to that of the body mass [$x(t_d) = X(t_d)$]. This moment is called "damper-separation," [$t = t_d$]. After damper-separation, the spring that connects the damper mass to the body mass is eliminated, and the damper mass and the body mass are separated. The intervals t such that $t \le t_0$, $t_0 \le t \le t_b$, $t_b \le t \le t_d$, and $t_d \le t$ are called "Phase 0", "Phase 1", "Phase 2", and "Phase 3", respectively.

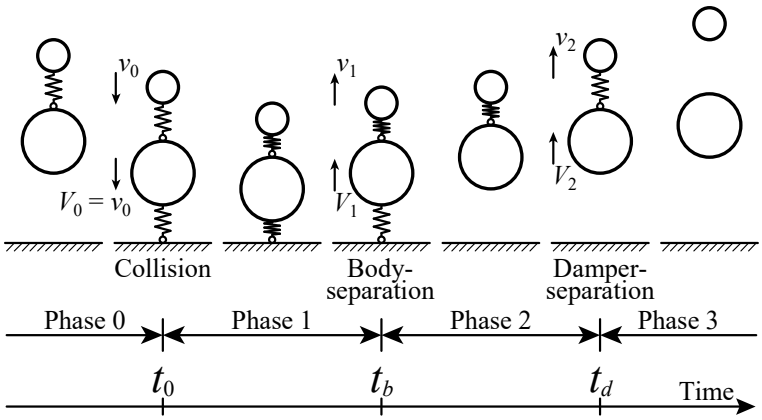

Figure 4. Schematic representation of the mechanical transitions of one-dimensional motion MEID collisions.

This study aims to derive optimal and sub-optimal MEID design parameters. The optimal design parameters control the body mass displacement and velocity after damper-separation to 0: $X(t_d) = 0$, $V(t_d) = 0$. This condition also implies that $t_b = t_d$ and $x(t_d) = 0$. These conditions are referred to as the "optimal condition" in this section. The

sub-optimal design parameter only controls the body mass velocity after damper-separation to 0: $V(t_d) = 0$, where $X(t_d) = x(t_d)$. These conditions were referred to as "sub-optimal condition" in this section.

2.2. Optimal design parameters

This section obtains the optimal design parameters by theoretical analyses and shows their typical responses by simulations.

2.2.1 Theoretical analyses

Optimal design parameters can be obtained by theoretical analyses of response of the model described in Fig. 3. The following equation describes the equation of motion in phase 1 in Fig.4:

$$\begin{aligned}\ddot{\boldsymbol{x}}(t) &= \begin{bmatrix} -k/m & k/m \\ k/M & -(k+K)/M \end{bmatrix} \boldsymbol{x}(t) \\ &= \begin{bmatrix} -\omega^2 & \omega^2 \\ \rho\omega^2 & -(\rho\omega^2 + \Omega^2) \end{bmatrix} \boldsymbol{x}(t),\ \boldsymbol{x}(t) = \begin{bmatrix} x(t) \\ X(t) \end{bmatrix}. \end{aligned} \tag{1}$$

where $\rho = m/M$, $\omega^2 = k/m$, $\Omega^2 = K/M$. The natural frequency of the system is summarized by the following expression:

$$\omega_{\pm}^2 = \frac{1}{2}\left[(\rho+1)\omega^2 + \Omega^2 \pm \sqrt{\left\{(\rho+1)\omega^2 + \Omega^2\right\}^2 - 4\omega^2\Omega^2} \right]. \tag{2}$$

Here, ω_- and ω_+ denote to first and second mode of the system vibration, respectively. By using the above equations and initial condition of phase 1, the solution of the system is described by the following expression:

$$\boldsymbol{x}(t) = v_0 \left\{ \sigma_- \begin{bmatrix} \varepsilon_- \\ 1 \end{bmatrix} \sin(\omega_- t) + \sigma_+ \begin{bmatrix} \varepsilon_+ \\ 1 \end{bmatrix} \sin(\omega_+ t) \right\}, \tag{3}$$

$$\sigma_{\pm} = \pm \frac{\omega_{\pm}^2 - (\rho+1)\omega^2}{\omega_{\pm}(\omega_+^2 - \omega_-^2)},\ \varepsilon_{\pm} = \frac{\omega_{\pm}^2 - \omega^2}{\rho\omega^2},\ \omega_+ \neq \omega_-. \tag{4}$$

When the system satisfies the optimal conditions, equation (3) may be expressed as the following equation:

$$\begin{bmatrix} \sigma_- & \sigma_+ \\ \sigma_-\varepsilon_- & \sigma_+\varepsilon_+ \end{bmatrix} \begin{bmatrix} \sin(\omega_- t) \\ \sin(\omega_+ t) \end{bmatrix} = \begin{bmatrix} 0 \\ 0 \end{bmatrix}. \tag{5}$$

Equation (5) is satisfied when $\sin(\omega_- t) = \sin(\omega_+ t) = 0$. Then, the optimal conditions also specifies that $V(t_d) = 0$. Here, $\gamma_{\pm}$ is defined as $\gamma_+ = \cos(\omega_+ t)$, $\gamma_- = \cos(\omega_- t)$. In order to satisfy Equation (5), the combinations of $\gamma_{\pm}$ include $(\gamma_+, \gamma_-) = (1, 1), (1, -1), (-1, 1), (-1, -1)$. The possible combinations that meet the optimal conditions include $(\gamma_+, \gamma_-) = (-1, 1), (1, -1)$. This results in the equation, $(\rho+1)\omega^2 = \Omega^2$; therefore,

$$\lambda = \frac{1}{\sqrt{\rho + 1}}, \tag{6}$$

by introducing $\lambda = \omega/\Omega$. Additionally, (γ_+,γ_-) = (-1, 1), (1, -1), $\omega_- t$ and $\omega_+ t$ can be described as $\omega_- t = n\pi$, $\omega_+ t = (n + [2p - 1])\,\pi$, where n, p are natural numbers. From equations (2) and (6), the mass ratio ρ can be specified by the following equation:

$$\rho = \left[\frac{(2n + 2p - 1)(2p - 1)}{2n(n + 2p - 1)}\right]^2. \tag{7}$$

Here, natural numbers n and p denote the first and second mode wave numbers, respectively. In the object-wall-collision problem, with optimal conditions, the possible first mode wave number in phase 1 is π, i.e., n = 1. Other cases indicated that damper-separation occurred before or after body-separation [$t_d < t_b$ or $t_b < t_d$].

2.2.2 Simulations

This subsection shows typical responses of the MEID model of a one-dimensional collision, tuned with the optimal parameters. The responses are shown in figure 5. This study assumed the case with n = 1 and p = 1 as the representative optimal parameters. Hence, this resulted in the simplest response with the lightest damper mass.

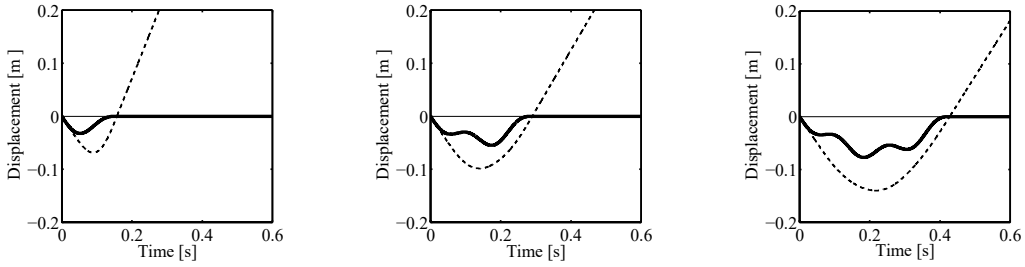

(a) n = 1, p = 1, m = 0.56 kg, k = 360 N/m

(b) n = 1, p = 2, m = 3.5 kg, k = 779 N/m

(c) n = 1, p = 3, m = 8.5 kg, k = 895 N/m

Figure 5. Typical responses of an optimal MEID in one-dimensional motion.

(v_0 = -1 m/s, M = 1 kg, K = 1 kN/m, **bold**: displacement of the body mass; thin-dashed: displacement of the damper mass)

2.3. Sub-optimal design parameters

This section obtains the sub-optimal design parameters by theoretical analyses and shows its typical response by simulations.

2.3.1 Theoretical analyses

Sub-optimal design parameters can be obtained by theoretical analyses based on appropriate assumption. The optimal condition consisted of the following three restrictions: $X(t_1) = 0$, $x(t_1) = 0$, and $V(t_1) = 0$. As a result, there was one point for optimal

parameters in a ρ-λ space, if the natural number was set as $n = 1$ and $p = 1$. By relaxing a restriction, the sub-optimal condition consisted of the following two restrictions: $X(t_2) = x(t_2)$, $V(t_2) = 0$. Thus, the sub-optimal parameters could be represented as a curve in the ρ-λ space. The parameters are obtained by simulations so that they are termed simulation-based sub-optimal parameters. Moreover, this study approximates the sub-optimal condition by assuming that the damper mass natural frequency is sufficiently small in order to simplify the parameter relation of the sub-optimal condition. This subsection derived the approximated sub-optimal parameter curve, which is termed analytically-obtained sub-optimal parameters curve.

Furthermore, the relationship between t_b and t_d varies based on the dynamics of the system. For example, collision and body-separation possibly occurred N times before damper-separation for a non-negative integer N. This study classifies collision vibration into the modes denoting "mode N" with respect to every N.

Figure 6 shows exemplary representations of collision vibration modes. Fig. 6 (A) shows "Mode 0" in which damper-separation occurred before body-separation. Fig. 6 (B) shows "Mode 1a," in which damper-separation occurs after body separation, and body velocity after the damper-separation is positive. Fig. 6 (C) shows "Mode 1b" in which damper-separation occurs after body separation, and body velocity after damper-separation is negative. Thus, boundary line between mode 1a and 1b corresponds to the optimal parameters at which the body velocity was zero. Fig. 6 (D) shows "Mode 2" in which the second collision occurs before damper separation. Fig. 6 (E) shows "Mode 3" in which second collision and second body-separation occurs before damper-separation. The higher modes in which the number of collisions and/or body-separations occurs three times or more are also observed in the parameter space.

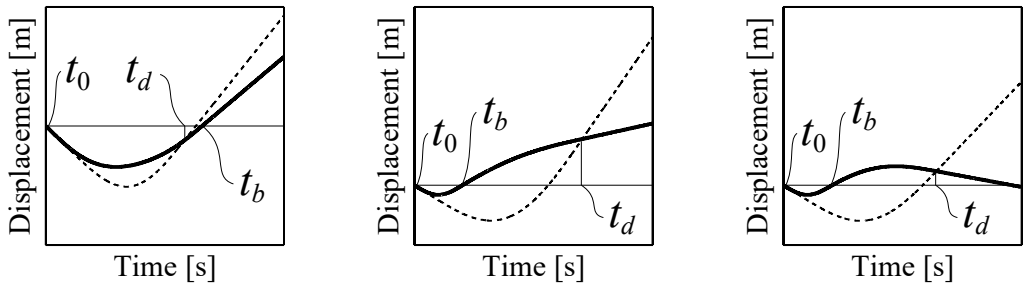

(A) Mode 0 ($\rho = 0.5, \lambda = 1.5$)

(B) Mode 1a ($\rho = 0.2, \lambda = 0.3$)

(C) Mode 1b ($\rho = 0.5, \lambda = 0.3$)

(D) Mode 2 ($\rho = 0.9, \lambda = 0.3$)

(E) Mode 3 ($\rho = 1.5, \lambda = 0.3$)

Figure 6. Schematic representations of one-dimensional collision vibration modes. (**bold**: displacement of the body mass; thin-dashed: displacement of the damper mass)

Figure 7 summarizes actual collision vibration modes variation according to the system parameters. In conditions involving smaller ρ and λ values, the collision phenomenon results in modes 1a and 1b. The boundary line between mode 1a and 1b corresponds to the optimal parameters of the object-wall-collision problem, which controls body mass velocity after damper-separation to 0. In heavier ρ and smaller λ condition, collision and body-separation easily occurred several times, i.e., at higher modes. In the higher λ condition, damper-separation possibly occurred before body-separation.

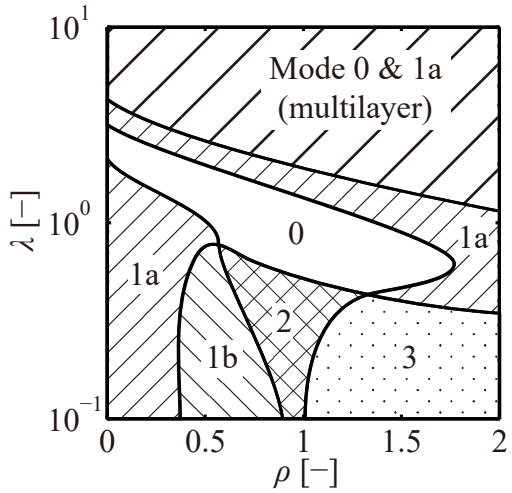

Figure 7. MEID one-dimensional collision vibration modes. (M = 1 kg, K = 1 kN/m, v_0 = 1 m/s)

This study focused on Mode 1 for purposes of simplicity. The collision vibration mode of the system can be tuned to Mode 1 without difficulty by choosing the system parameters. The design target of the analysis involved suppressing body mass velocity to approximately zero after damper-separation [$V(t_2) = 0$]. This section derives the sub-optimal parameters indicated by a boundary line between modes 1a and 1b by reasonable approximation.

In this section, Mode 1a and 1b were assumed, i.e., in smaller ρ and λ. This condition indicated that a damper mass and spring effect were sufficiently small. Given this assumption, the single mass collision problem and MEID collision problem were compared. Figure 8 shows the comparison. In the single mass collision problem, the following conservation laws are applied:

$$Mv_0 + \overline{P} = Mv_1, \frac{1}{2}Mv_0^2 = \frac{1}{2}Mv_1^2, \tag{8}$$

where $\overline{P}$ denotes the collision momentum from the wall. From equation (8), the collision momentum $\overline{P}$ can be calculated according to the following expression:

$$\overline{P} = 2Mv_0. \tag{9}$$

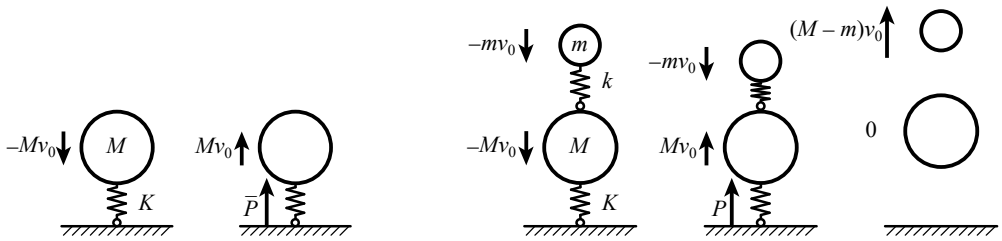

Figure 8. Momentum transfer of a mass and MEID collision.

The assumption that "ρ and λ are sufficiently small" was then considered. The collision impact to the body mass of the MEID collision P was similar to that of a mass collision $\bar{P}$ [$P \approx \bar{P}$]. This assumption simplified analysis. Initial momentum of a damper mass and a body mass are denoted by $-mv_0$ and $-Mv_0$, respectively. The body mass takes the collision impact $P = 2Mv_0$, and hence the body mass momentum becomes Mv_0. However, the damper mass momentum (denoted by$-mv_0$) did not change because the spring effect was sufficiently small. The total momentum of the system is denoted by $(M - m)v_0$. In the sub-optimal condition, the total momentum of the system was transferred to the damper mass such that the damper mass velocity after the damper separation is $(M - m)/m \cdot v_0$. The following expression was derived by using the energy conservation law:

$$\frac{1}{2}(M+m)v_0^2 = \frac{1}{2}m\left[\frac{M-m}{m}v_0\right]^2. \tag{10}$$

The mass ratio may be obtained by the following expression after solving equation (10):

$$\rho = \frac{m}{M} = \frac{1}{3}. \tag{11}$$

This is the sub-optimal parameter of MEID in one-dimensional motion.

2.3.2 Simulations

This subsection shows a typical response of the MEID model of a one-dimensional collision, tuned with the sub-optimal parameters. Here, initial velocities of both the body mass and the damper mass are – 1 m/s. Initial displacements of them are 0 m. The response is shown in figure 9. The body mass velocity becomes zero but displacement does not keep zero.

Figure 10 summarized optimal, analytically-obtained sub-optimal and simulation-based sub-optimal parameters. The optimal parameters solved in Eqs. (6) and (7) are definitely located at a point in the parameter space and coincides with a terminated point of the simulation-based sub-optimal parameter curve as a boundary between Mode 1a and 1b in Figure 7. It is noted that the termination is caused by the appearance of Mode 0. The result further shows that the analytically-obtained sub-optimal parameter set derived in Eq. (11) does not include the optimal parameter point, meaning

that both the displacement and the velocity do not vanish completely in the analytically-obtained sub-optimal condition. It is however worthy of note that the analytically-obtained sub-optimal line converges to the simulation-based sub-optimal curve as $\lambda \to 0$, which is consistent with the assumption of the approximation.

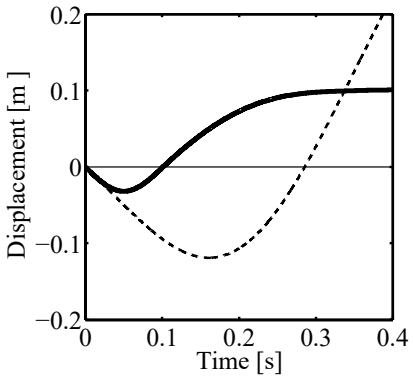

Figure 9. An example of the time response of analytically-obtained sub-optimal parameters
(**bold**: displacement of the body mass; thin-dashed: displacement of the damper mass)
(M = 1 kg, K = 1 kN/m, ρ = 1/3, λ = 0.3).

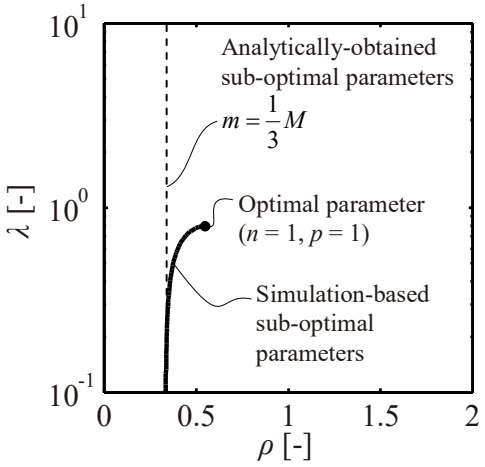

Figure 10. Optimal parameters, analytically-obtained sub-optimal parameters and simulation-based sub-optimal parameters.

2.4. Robustness evaluation

This section verifies the robustness of MEIDs that were tuned in optimal and sub-optimal parameters. This was performed by varying the stiffness of a wall and evaluating the body mass velocity. Since this paper focuses on momentum exchange using MEIDs for controlling shock response of the first landing impact, the important parameters are mass and spring constant. In a practical situation, effective stiffness of a wall is not correctly known before landing because of incomplete ground-condition estimation. Thus, this paper set mass as a known value and focuses on robustness

against variation of stiffness of a wall rather than a viscosity. Figure 11 shows the simulation results. The results indicated that the optimal-tuned MEID performance was dramatically reduced by the wall stiffness K variation. Conversely, the sub-optimal-tuned MEID performance was especially stable in the area where the wall stiffness (denoted by K) was hard. However, the performance was degraded in the lower K area because the approximation that "λ is sufficiently small" did not fit in this area. Based on this discussion, the MEID should be designed with the optimal parameter in the case where the wall stiffness was precisely obtained. In contrast, the MEID should be designed with the sub-optimal parameter in the case in which the wall stiffness is unclear.

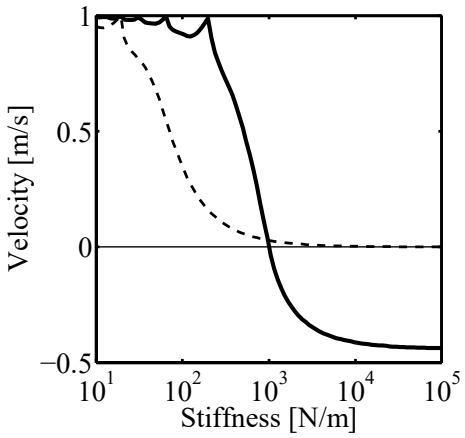

Figure 11. Robustness evaluation of the optimal MEIDs and sub-optimal tuned MEIDs

(M = 1 kg, **bold**: MEID tuned in the optimal parameter for K = 1 kN/m; thin-dashed: MEID tuned in the sub-optimal parameter).

3. MEID design for two-dimensional motion

3.1. Design parameters of a MEID in two-dimensional motion

The aim of this section included deriving theoretical MEID design methodology, which suppressed both translational and rotational motions after collision. This parameter design was similar to analytically-obtained sub-optimal parameters in one-dimensional motion since the design focused on translational and rotational velocities. From this viewpoint, the momentum transfer discussion in the previous section was expanded to include two-dimensional motion in this section.

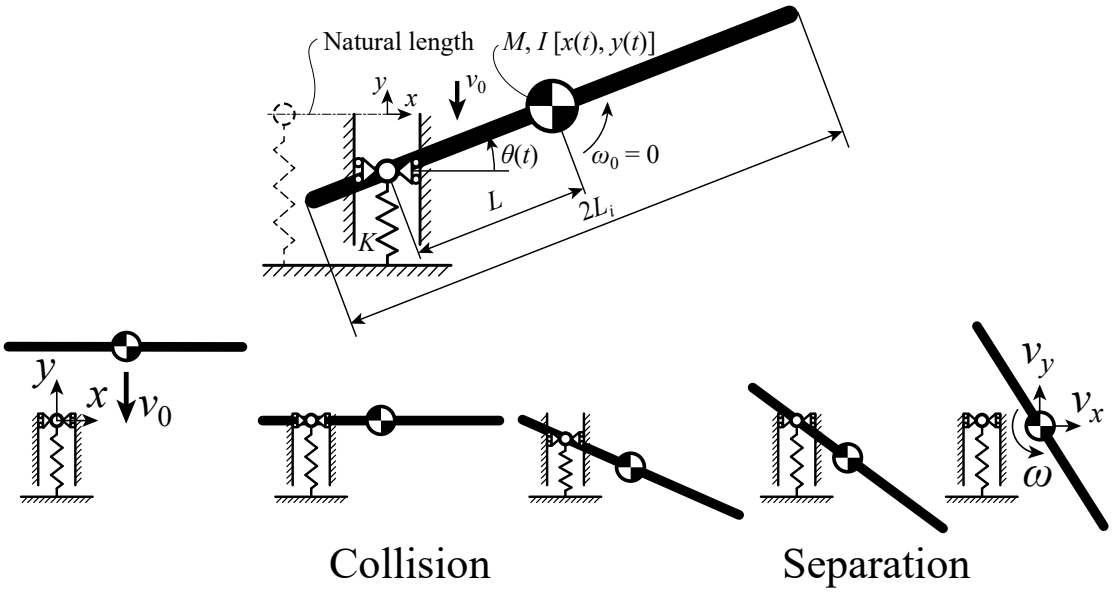

Figure 12. Object-wall-collision of a mass.

This section first introduced a two-dimensional collision model of a mass as shown in Fig. 12 to discuss the design methodology. In the collision model, a body mass (denoted by M) with an inertia of moment (denoted by I) collided with a wall. The body mass was assumed as a bar with a length (denoted by $2L_i$). Thus, its moment of inertia is given by $I = ML_i^2/3$. A spring element described the contact force, which was normal to the wall and was between the body mass and the wall during the period from the collision to the body separation. The force parallel to the wall was described by a constraint. Thus, the contact point did not slide in a direction parallel to the wall. This collision phenomenon was referred to as the object-wall-collision in this study.

The momentum conservation law, angular momentum conservation law, and energy conservation law are derived through the collision by the following equations:

$$Mv_0 + \overline{P} = M\overline{v}_1 \tag{12}$$

$$I\omega_0 - \overline{P}L = I\overline{\omega}_1 \tag{13}$$

$$\frac{1}{2}Mv_0^2 = \frac{1}{2}M\overline{v}_1^2 + \frac{1}{2}I\overline{\omega}_1^2 \tag{14}$$

where v_0 and ω_0 (= 0) denote the initial velocity and angular velocity, respectively; $\overline{v}_1$ and $\overline{\omega}_1$ denote velocity and angular velocity after collision, respectively; and $\overline{P}$ denotes the collision momentum from the wall to the body of the object-wall-collision model without MEID. This discussion ignored the force parallel to the wall for the sake of simplicity. Furthermore, $\overline{P}$ was calculated based on equations (12)–(14) and was given by the following equation:

$$\overline{P} = \frac{-2MI}{I + ML^2} v_0 \tag{15}$$

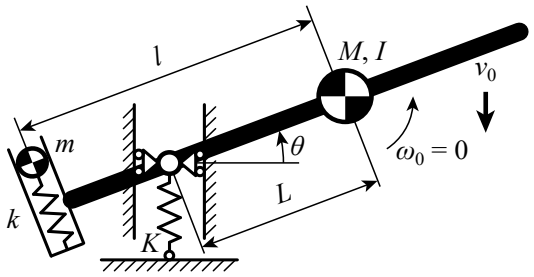

Figure 13. Two-dimensional collision model of MEID.

Following this, the object-wall-collision model with MEID as shown in Fig. 13 was discussed. The model consists of two masses. Dynamics of a model that is composed of multiple masses was discussed in multibody dynamics fields (Kane, 1961). This study simply discusses the dynamics on the bases of conservation laws to derive the analytically-obtained sub-optimal design parameters. The following equations summarize the conservation laws:

$$(M + m)v_0 + P = MV_1 + mv_1 \tag{16}$$

$$I\omega_0 - P\left(L - \frac{m}{M+m}l\right) = -mv_1\left(\frac{M}{M+m}l\right) + MV_1\left(\frac{m}{M+m}l\right) + I\omega_1 \tag{17}$$

$$\frac{1}{2}(M+m)v_0^2 = \frac{1}{2}MV_1^2 + \frac{1}{2}mv_1^2 + \frac{1}{2}I\omega_1^2 \tag{18}$$

where V_1 and v_1 denote the body and the damper mass velocity after collision, respectively. Furthermore, ω_1 denotes the body mass angular velocity after collision and P denotes the collision momentum from the wall to the body of the object-wall-collision model with MEID. This section derived the optimal MEID design parameters (denoted by m, k and l), which suppressed the body velocity and angular velocity after collision ($V_1 = 0$, $\omega_1 = 0$) based on equations (15)–(18).

In this section, it was assumed that the MEID spring stiffness (denoted by k) was much smaller than that of wall stiffness (denoted by K). Additionally, the damper mass (denoted by m) was assumed to be much smaller than the body mass (denoted by M). These assumptions were the same as those in the one-dimensional motion study; that is, "ρ and λ are sufficiently small." Thus, the collision momentum of a mass (denoted by $\overline{P}$) was assumed as similar to the collision momentum with MEID P [$P \approx \overline{P}$]. Under the assumptions ($V_1 = 0$, $\omega_1 = 0$, $P \approx \overline{P}$), the analytically-obtained sub-optimal MEID parameters were derived as the following equations.

$$\rho = \frac{m}{M} = \frac{\left(I - ML^2\right)^2}{\left(I + ML^2\right)\left(3I - ML^2\right)} \tag{19}$$

$$\nu = \frac{l}{L} = \frac{2I}{I - ML^2} \tag{20}$$

The motion of the body of the object-wall-collision model could be suppressed with the MEID by using the above analytically-obtained sub-optimal parameters. However, the body inertia of moment (denoted by I) must exceed ML^2. This optimization cannot be applied when I is smaller than ML^2.

3.2. Simulation studies

This section discussed the effectiveness and the robustness of the optimal design parameters obtained in the previous section.

3.2.1 Effectiveness of the theoretical results

First, the motions of the object-wall-collision models without MEID and with the optimal MEID were compared. Table 1 and 2 summarize the model parameters of the model without MEID and the model with the optimal MEID, respectively. In this section, initial displacement and angular displacement of the body are 0 m. MEID spring initial extension amount is also 0 m. Initial rotational velocity is 0 rad/s. Initial horizontal velocity is 0 m/s, vertical velocity is – 1 m/s.

The corresponding time responses are shown in Figures 14 and 15, respectively. By applying the analytically-obtained sub-optimal parameters, translational and rotational velocities after collision were approximately suppressed in a practical manner.

Table 1. Parameter of the object-wall-collision model without MEID.

Parameter	**Symbol**	**Value**	**Unit**
Body mass	M	1	kg
Inertia of the body	I	5	kg m^2
Stiffness of the wall	K	1	N/m
Displacement of the collision point	L	1	m

Table 2. Parameter of the object-wall-collision model with sub-optimal MEID.

Parameter	**Symbol**	**Value**	**Unit**
Body mass	M	1	kg

Parameter	Symbol	Value	Unit
Inertia of the body	I	5	kg m^2
Stiffness of the wall	K	1	N/m
Displacement of the collision point	L	1	m
Damper mass (sub-optimal designed)	m	0.19	kg
Damper mass attachment position (sub-optimal designed)	l	2.5	m

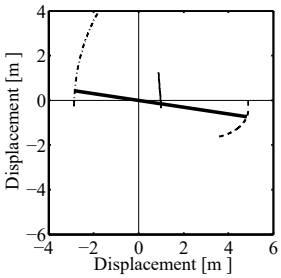

(a) Trajectory

(**bold**: body mass attitude at the moment of the end of the collision; thin: trajectory of the gravity center; dashed: trajectory of the right-end of the body; dot-dashed: trajectory of the left-end of the body)

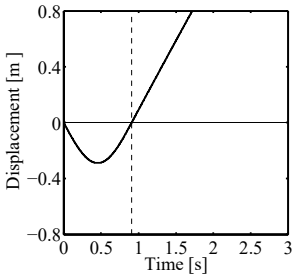

(b) Displacement of the body contact point

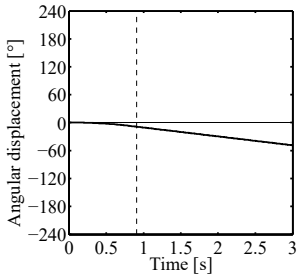

(c) Angular displacement of the body

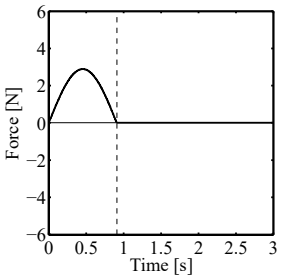

(d) Force of collision

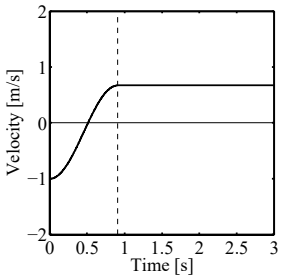

(e) Translational velocity of the body

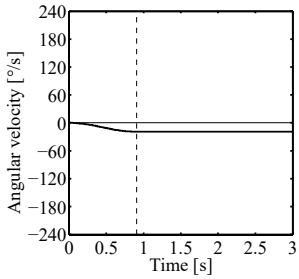

(f) Rotational velocity of the body

Figure 14. Time responses of the object-wall-collision model without MEID.

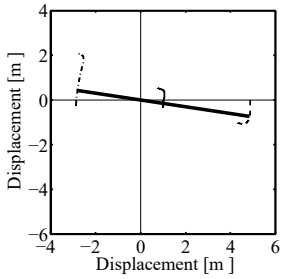

(a) Trajectory

(**bold**: body mass attitude at the moment of the end of the collision; thin: trajectory of the gravity center; dashed: trajectory of the right-end of the body; dot-dashed: trajectory of the left-end of the body)

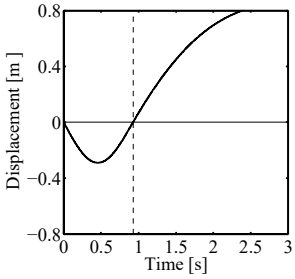

(b) Displacement of the body contact point

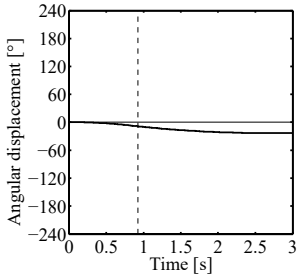

(c) Angular displacement of the body

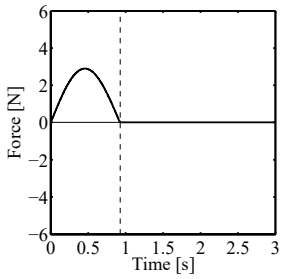

(d) Force of collision

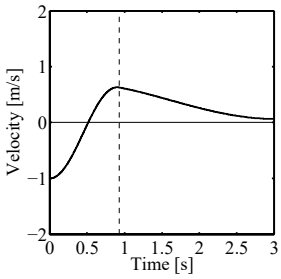

(e) Translational velocity of the body

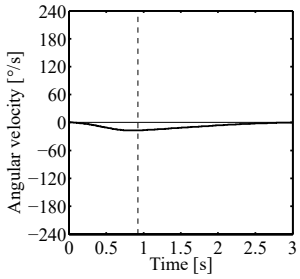

(f) Rotational velocity of the body

Figure 15. Time responses of the object-wall-collision model with analytically-obtained sub-optimal MEID.

3.2.2 Simulation-based optimal parameters

This section compared the optimal parameters obtained by simulations (Kushida and Hara, 2015) and the analytically-obtained sub-optimal parameters in section 3.1. Initial conditions of this simulations are same as those of Subsection 3.2.1. The body mass translational and rotational velocity after the damper mass separation are evaluated.

Figure 16 summarizes the comparison. The bold line indicates the relationship that suppressed the rotational velocity (denoted by M) at the moment of additional mass (denoted by m) separation to zero. The thin line indicates the relationship that suppressed the translational velocity (denoted by M) at the moment of additional mass separation to zero. The parameters that suppressed both the rotational and translational velocities of mass M were l = 2.4 m and m = 0.21 kg. These values were similar to the

theoretical values (l = 2.5 m and m = 0.19 kg). The difference was considered as the result from the assumption $P \approx \overline{P}$.

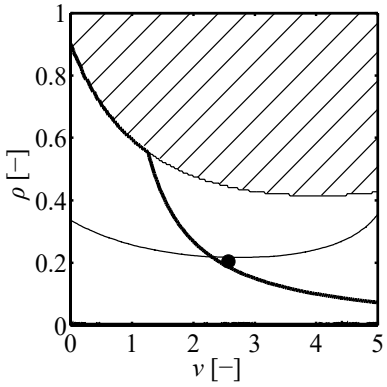

Figure 16. Comparison of simulation-based optimal parameters and the analytically-obtained sub-optimal parameters.

(**bold**: parameters that suppress rotational velocity of M at the moment of additional mass m separation to zero;
thin: parameters that suppress translational velocity of M at the moment of additional mass m separation to zero;
dot: theoretically obtained sub-optimal parameters).

3.2.3 Robustness of the sub-optimal parameters

Figure 17 shows the robustness of the sub-optimal parameters calculated by the theoretical analyses and simulation-based parameters with respect to the wall stiffness variation. Initial conditions of this simulations are same as those of Subsection 3.2.1. The body mass translational and rotational velocity after the damper mass separation are evaluated. The simulation-based parameters were tuned for K = 1 kN/m such that both translational and rotational velocities were controlled at the tuned point. Conversely, the sub-optimal parameters experienced some degradation at K = 1 kN/m. However, the sub-optimal parameter performances improved at higher values of K. If K becomes high, the assumption that "λ was sufficiently small" corresponded well and hence the results improved. These results indicated that MEID should be designed with the sub-optimal parameters with sufficiently small λ for the two-dimensional motion

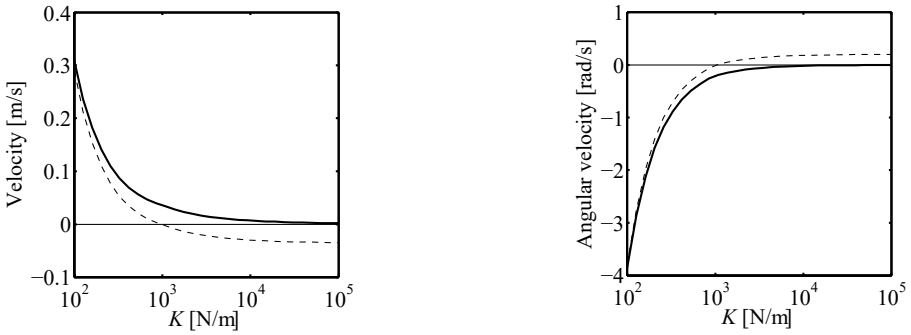

(a) Translational velocity of the body after separation

(b) Rotational velocity of the body after separation

Figure 17. Robustness of the sub-optimal parameters and simulation-based parameters with respect to the wall stiffness variation

(**bold**: sub-optimal parameters; thin-dashed: simulation-based parameters that are tuned for K = 1 kN/m)

4. Conclusion

This study has been systemized MEID design methodology for an object that collides with a wall. Damping the translational motion was theoretically analyzed by one-dimensional model. The optimal MEID parameters that controlled a body mass displacement and velocity to zero were solved explicitly. Additionally, analytically-obtained sub-optimal parameters that controlled only body mass velocity were derived using a practical approximation. The approximation assumed that the damper mass natural frequency was sufficiently small when compared to that of the body and the wall.

Even in the two-dimensional case allowing rotational motion, the analytically-obtained sub-optimal parameters to suppress both the translational and rotational velocities of the body mass were derived with a suitable approximation. The analytically-obtained sub-optimal parameters are obtained from the conservation laws of energy and momentum in the one-dimensional model and additionally the angular momentum in the two-dimensional model.

The velocity damping for inaccurate stiffness of the wall is an issue of the design in the landing problem for space mission. The robust settings of parameters which are adaptable to a wide range of stiffness are required, provided that the constitution of a wall material and the resulting stiffness are not estimated a priori. In this study, the robustness of MEIDs tuned in the optimal and sub-optimal parameters are compared to each other. The complete landing of the body mass with zero velocity is realized by the choice of the optimal parameter if the stiffness of the wall is known precisely, whereas the MEID with the sub-optimal parameters showed a better robustness compared to the MEID with the optimal parameters. Furthermore, the sub-optimal parameter performances improved if a good fit was obtained for the approximation for both the one-dimensional model and the two-dimensional model. Hence, a MEID with a strong

robustness is feasible by the design with the analytically-obtained sub-optimal parameters.

This systematic study will be a basis for future studies, involving an experimental study, actual implementation of MEIDs to the lunar/planetary exploration spacecraft, and derivation of the optimal parameters of MEIDs in two-dimensional motion. The results in this study theoretically summarized previous MEID studies, and the results obtained in this study significantly contribute to the actual implementation of MEIDs.

ACKNOWLEDGMENT

This work was supported in part by a Grant-in-Aid for Scientific Research (A) (Grant 26249023) from the Japan Society for the Promotion of Science. The authors would like to thank Masatsugu Otsuki and Yoji Yamada for their helpful instructions.

References

Bapat CN and Sankar S (1985a) Single unit impact damper in free and forced vibration. *Journal of Sound and Vibration* 99(1): 85-94.

Bapat CN and Sankar S (1985b) Multiunit impact damper – re-examined. *Journal of Sound and Vibration* 103(4): 457-469.

Cheng CC and Wang JY (2003) Free vibration analysis of a resilient impact damper. *International Journal of Mechanical Sciences* 45: 589-604.

Cheng J and Xu H (2006) Inner mass impact damper for attenuating structure vibration. *International Journal of Solids and Structures* 43: 5355-5369.

Dondo K and Noborio H (2008) Experiment and evaluation of multi-collision movement model using Newton's cradle *The Special Interest Group Technical Reports of IPSJ* 2008-EC-9: 29-36.

Duncan MR, Wassgren CR and Krousgrill CM (2005), The damping performance of a single particle impact damper. *Journal of Sound and Vibration* 286: 123-144.

Hara S, Ito R, Otsuki M, Yamada Y, Kubota T, Hashimoto T, Matsuhisa H and Yamada K (2011) Momentum-exchange-impact-damper-based shock response control for planetary exploration spacecraft. *Journal of Guidance Control and Dynamics* 34(6): 1828-1838.

Hara S, Watanabe T, Kushida Y, Otsuki M, Yamada Y, Matsuhisa H, Yamada K, Hashimoto T and Kubota T (2012) Study on landing response control of planetary exploration spacecraft based on momentum exchange principles. *Transactions of the JSME Series C* 78(792): 2781-2796.

Herrmann F and Schmälzle P (1981) Simple explanation of a well-known collision experiment. *American Journal of Physics* 49: 761-764.

Herrmann F and Seitz M (1982) How does the ball-chain work? *American Journal of Physics* 50: 977-981.

Hufenbach B, Laurini KC, Satoh N, Piedboeuf JC, Lange C, Martinez R, Wargo M, Hill J and Spiero F (2013) The 2nd iteration of the ISECG global exploration roadmap. *Proceedings of the 64th International Astronautical Congress* IAC-13 B3 1: 8x16946.

Kane T R (1961) Dynamics of Nonholonomic Systems. *Journal of Applied Mechanics* 28: 29-36.

Kitazono K, Sato E and Sawai S (2010) Application of aluminum foam for landing gear of smart lander. *Proceedings of 54th Space Science and Technology Conference*: JSASS-2010-4218.

Kushida Y (2013) Shock response control using a MEID mechanism – consideration of a multi-legged landing gear system –. *Proceedings of 56th Japan Joint Automatic Control Conference*: 266-269.

Kushida Y and Hara S (2015) Dynamics of a two-mass-spring system which is separated by external input. *Proceedings of the 2015 IEEE International Conference on Mechatronics (ICM)*: 472-477.

Kushida Y, Hara S, Otsuki M and Yamada Y (2013a) Shock response control using MEIDs –consideration of a single-axis falling type problem–. *Transactions of the JSASS Aerospace Technology Japan* 10(ists28): Pd_67-Pd_75.

Kushida Y, Hara S, Otsuki M, Yamada Y, Hashimoto T and Kubota T (2013b) Robust landing gear system based on a hybrid momentum exchange impact damper. *Journal of Guidance Control and Dynamics* 36(3): 776-789.

Lu Z, Masri SF and Lu X (2011a) Parametric studies of the performance of particle dampers under harmonic excitation. *Structural Control and Health Monitoring* 18(1): 79-98.

Lu Z, Masri SF and Lu X (2011b) Studies of the performance of particle dampers attached to a two-degree-of-freedom system under random excitation. *Journal of Vibration and Control* 17(10): 1454-1471.

Lu Z, Lu X, Jiang H and Masri SF (2014) Discrete element method simulation and experimental validation of particle damper system. *Engineering Computations* 31(4): 810-823.

Lu Z, Chen X, Zhang D and Dai K (2016a) Experimental and analytical study on the performance of particle tuned mass dampers under seismic excitation. *Earthquake Engineering and Structural Dynamics* DOI: 10.1002/eqe.2826.

Lu Z, Wang D, Masri SF and Lu X (2016b) An experimental study of vibration control of wind-excited high-rise buildings using particle tuned mass dampers. *Smart Structures and Systems* 18(1): 93-115.

Lu Z, Wang D and Zhou Y (2017) Experimental parametric study on wind-induced vibration control of particle tuned mass damper on a benchmark high-rise building. *The Structural Design of Tall and Special Buildings* DOI: 10.1002/tal.1359

Nyawako DS and Reynolds P (2015) Observer-based controller for floor vibration control with optimization algorithms. *Journal of Vibration and Control*. Epub ahead of print 3 June 2015. DOI:10.1177/1077546315581229.

Oda M and Hukatsu K (1979) The longitudinal impact of a bar accompanied by lateral deformation. *Transactions of the JSME Series A* 45(397): 1098-1103.

Saeki M (2005) Analytical study of multi-particle damping. *Journal of Sound and Vibration* 281: 1133-1144.

Son L, Hara S, Yamada K and Matsuhisa H (2010) Experiment of shock vibration control using active momentum exchange impact damper. *Journal of Vibration and Control* 16(1): 49-64.

Son L, Kawachi M, Matsuhisa H and Utsuno H (2007) Reducing floor impact vibration and sound using a momentum exchange impact damper. *Journal of System Design and Dynamics* 1(1): 14-26.

Son L, Matsuhisa H, and Utsuno H (2008a) Energy transfer in a three body momentum exchange impact damper. *Journal of System Design and Dynamics* 2(1): 425-441

Son L, Yamada K, Hara S, Utsuno H and Matsuhisa H (2008b) Reduction of floor shock vibration by active momentum exchange impact damper. *Journal of System Design and Dynamics* 2(4): 930-939.

Thomas MD and Sadek MM (1974) The effectiveness of the impact damper with a spring-supported auxiliary mass. Journal Mechanical Engineering Science 16(2): 109-116.

Watanabe T, Hara S and Otsuki M (2014) Study on passive momentum exchange landing gear using two-dimensional analysis. *Acta Astronautica* 105(2): 407-416.